RSC Advances

PAPER

View Article Online
View Journal | View Issue

Cite this: *RSC Adv.*, 2020, **10**, 29326

Ultrafine Co_3O_4 nanolayer-shelled CoWP nanowire array: a bifunctional electrocatalyst for overall water splitting†

Lili Zhang,‡[ab] Tingting Zhang,‡[b] Kaiqing Dai,[a] Liqing Zhao,[a] Qinghe Wei,[a] Bing Zhang [a] and Xu Xiang *[b]

Received 8th July 2020
Accepted 22nd July 2020

DOI: 10.1039/d0ra05950a

rsc.li/rsc-advances

The development of bifunctional electrocatalysts based on highly efficient non-noble metals is pivotal for overall water splitting. Here, a composite electrode of Co_3O_4@CoWP is synthesized, where an ultrathin layer composed of Co_3O_4 nanoparticles is grown on CoWP nanowires supported on a carbon cloth (CC). The Co_3O_4@CoWP/CC electrode exhibits excellent electrocatalytic activity and improved kinetics towards both the oxygen and hydrogen evolution reactions (OER and HER). The Co_3O_4@CoWP/CC electrode achieves a current density of 10 mA cm^{-2} at a low overpotential of 269 mV for the OER and −10 mA cm^{-2} at 118 mV for the HER in 1.0 M KOH solution. The voltage applied to a two-electrode water electrolyzer for overall water splitting, while employing the Co_3O_4@CoWP/CC electrode as both an anode and a cathode, in order to reach a current density of 10 mA cm^{-2}, is 1.61 V, which is better than that for the majority of reported non-noble electrocatalysts. Moreover, the Co_3O_4@CoWP/CC electrode exhibits good stability over 24 h with slight attenuation. The electrode benefits from the enhanced adsorption of oxygen intermediates on Co_3O_4 during the OER, the increased ability for water dissociation and the optimized H adsorption/desorption ability of CoWP nanowires during the HER. This study provides a feasible approach for cost-effective and high-performance non-noble metal bifunctional catalysts for overall water electrolysis.

Introduction

Hydrogen has become a convenient and inevitable alternative for new energy consumption in recent years, due to its environmental friendliness, sustainability, and superior gravimetric energy density.[1] Among the various hydrogen production technologies, the effective utilization of electrocatalytic water splitting is expected to provide a viable method for 'clean' hydrogen production.[2,3] It is generally believed that the overall electrocatalytic water splitting process consists of two half-reactions of the oxygen evolution reaction (OER) and the hydrogen evolution reaction (HER).[4] The efficiency and kinetics of both these reactions rely strongly on the electrocatalysts used.[5] It has been demonstrated in many studies that the noble metal Pt and noble metal oxides (IrO_2 and RuO_2) can achieve significantly higher electrocatalytic activities for HER and OER, respectively. The high cost, low storage, and single-functionality of these noble metal-based electrocatalysts strongly hinder their widespread applications.[6–8] Thus, the rational design and exploitation of cost-efficient and electroactive transition metal-based catalysts with bifunctionality is highly attractive for overall water splitting.

Transition metal phosphides (TMPs, M = W, Ni, Co, Mo, Fe, and Cu) have been reported as efficient catalysts for the HER due to their high electrical conductivity, metalloid characteristics, and good electrocatalytic activities.[9–15] Furthermore, the phosphorus element in TMPs not only has the ability to trap protons, but it also exhibits good affinity to the reaction intermediates, thus facilitating the HER reaction dynamics.[16] However, while TMPs generally exhibit excellent electrochemical performances in acidic electrolytes, they perform poorly in alkaline electrolytes.[9,17] Electrolytic hydrogen evolution in alkaline electrolytes has been carried out successfully for many years and high-purity hydrogen (approximately 100%) can be obtained with moderate energy consumption. Therefore, considering the practical applications, it appears to be more urgent to explore high-efficiency TMP catalysts for HER in alkaline media. It has been found that the HER activities of TMPs in alkaline conditions can be improved by doping with an additional metal to tune their crystal and electronic structures.[16] For example, NiCoP,[16] FeCoP, CoMoP, WCoP, and CoFeP[18–21]

[a]School of Chemical Engineering, Zhengzhou University, Zhengzhou 450001, P. R. China

[b]State Key Laboratory of Chemical Resource Engineering, Beijing University of Chemical Technology, 15 Beisanhuan East Road, Beijing 100029, PR China. E-mail: xiangxu@mail.buct.edu.cn

† Electronic supplementary information (ESI) available. See DOI: 10.1039/d0ra05950a

‡ These authors contributed equally.

have been confirmed to show better HER activities than the corresponding single-metal phosphides in alkaline electrolytes. The heterogeneous metal-doping of TMPs can effectively lower the energy barrier of H adsorption, facilitate electron transfer, and provide abundant active sites, thus significantly improving HER catalytic performance in alkaline electrolytes.[22]

Even though transition metal-doped TMPs display excellent HER performance, their unsatisfactory OER performance greatly hinders their practical application for overall water splitting. Some studies have indicated that the integration of inexpensive and efficient OER and HER catalysts into a compatible hybrid is a viable route for obtaining an excellent bifunctional catalyst for electrochemical water splitting.[23,24] The modified electronic structure, the synergistic effect between the two components, and the interfacial defective sites in the hybrid give rise to improved properties. The spinel structure of Co_3O_4 can be considered to be a promising electrocatalyst for the OER in alkaline media, because of its high redox activity, abundant resources and low price.[25,26] Moreover, Co_3O_4 also shows good electrocatalytic performance towards the HER.[27] Thus, it is reasonable to expect that the hybrid TMPs/Co_3O_4 catalyst will be an efficient and practical bifunctional electrocatalyst for overall water splitting.

Taking the aforementioned concepts into account, and with the aim of constructing efficient bifunctional catalysts for overall water splitting, cobalt-doped tungsten phosphide (CoWP) nanowires self-supported on carbon cloth (CC) with an ultrathin layer of Co_3O_4 nanoparticles as the shell (named Co_3O_4@CoWP/CC) were designed and prepared by a hydrothermal method involving phosphidation and annealing, and they served as efficient free-standing bifunctional electrocatalysts for water electrolysis. The results showed that the CoWP nanowire array can effectively prevent the Co_3O_4 nanoparticles from agglomerating and that the Co_3O_4 ultrafine nanoparticles are distributed evenly on the nanowire. Benefiting from the peculiar structure of Co_3O_4@CoWP/CC and the synergy between Co_3O_4 and CoWP, the designed Co_3O_4@CoWP/CC electrode showcases impressive electrocatalytic properties for both OER and HER with small overpotentials of 269 and 118 mV needed to deliver a current density of 10 mA cm^{-2} in 1.0 M KOH, respectively. The fabricated Co_3O_4@CoWP/CC‖Co_3O_4@CoWP/CC electrolyzer only requires a low cell voltage of 1.61 V to drive the overall water splitting process to generate a current density of 10 mA cm^{-2}.

Experimental

Materials

Commercial Pt/C (5 wt%), cobalt nitrate hexahydrate ($Co(NO_3)_2 \cdot 6H_2O$, 99%), sodium tungstate dehydrate ($Na_2WO_4 \cdot 2H_2O$, 99%), sodium hypophosphite (NaH_2PO_2, 99%), ruthenium dioxide (RuO_2, 99%), hydrochloric acid (HCl, 37 wt%), potassium hydroxide (KOH, 85%) and oxalic acid ($H_2C_2O_4$, 99%) were purchased from Aladdin Ltd (China). Carbon cloth (WOS1009) was obtained from Taiwan CeTech Co., Ltd. Ammonium sulfate ($(NH_4)_2SO_4$, 99%) and cyclohexane (98%) were purchased from Kermel Co., Ltd. Octadecylamine (ODA, 97%) was obtained from Macklin Chemical Reagent Co., Ltd.

Synthesis of CoWP/CC

The cobalt and tungsten oxide nanowires on carbon cloth (CoWO/CC) were synthesized by a simple hydrothermal procedure according to previous studies.[15] Typically, $Na_2WO_4 \cdot 2H_2O$ (12.5 mmol) was dissolved in deionized water (100 mL), and a 3.0 M HCl aqueous solution was subsequently slowly dropped into the solution until it reached a pH value of 1.2, forming a yellowish transparent solution. Then, $H_2C_2O_4$ (35 mmol) was added into the above solution and diluted to 250 mL, resulting in the H_2WO_4 precursor. Next, the H_2WO_4 precursor solution (70 mL), $(NH_4)_2SO_4$ (3.5 g) and $Co(NO_3)_2 \cdot 6H_2O$ (0.35 g) were mixed in a Teflon-lined autoclave (100 mL), and the mixture was stirred to obtain a homogeneous solution. Subsequently, a piece of carbon cloth (2 × 3 cm^2) that was ultrasonically cleaned by acetone, alcohol, and deionized water in succession, was placed into the autoclave, and then the hydrothermal process took place under 180 °C for 16 h. The CoWO/CC precursor was cleaned with deionized water and dried at 60 °C. Finally, the precursor was phosphatized using NaH_2PO_2 at 300 °C for 3 h under an inert atmosphere, and the product of CoWP/CC was obtained.

Synthesis of Co_3O_4@CoWP/CC

The modification of Co_3O_4 nanoparticles on CoWP/CC was carried out through the following steps.[28] Briefly, ethanol (30 mL) was mixed with $Co(NO_3)_2 \cdot 6H_2O$ (1.5 mmol) in a beaker to form a red solution. Subsequently, octadecenylamine (2 mL) with ethanol (10 mL) were added under stirring, obtaining a green solution. Next, the as-prepared mixture and CoWP/CC were transferred to a Teflon-lined autoclave (50 mL) and were kept at 180 °C for 12 h. The obtained product of Co_3O_4@CoWP/CC was rinsed with cyclohexane and ethanol repeatedly, and dried at 60 °C. The resulting hybrid was calcinated in air at 350 °C for 3 h. The sample loading amounts of CoWP/CC and Co_3O_4@CoWP/CC were determined by a microbalance to be 7.8 and 8.1 mg cm^{-2}, respectively. For comparison, the Co_3O_4 powder was obtained by the same hydrothermal process, but without CC. The powder of 8.1 mg cm^{-2} was post-coated on CC (denoted as Co_3O_4/CC).

Characterization

X-ray diffraction (XRD, Bruker D8 Advance, scan range of 3–80°) analysis was used to determine the crystal structures of the samples. X-ray photoelectron spectroscopy (XPS) analysis was carried out with an Escalab 250Xi electron spectrometer using MgKα radiation. Scanning electron microscopy (SEM) images were obtained using an Ultra 55Zeiss field emission scanning electron microscope. Transmission electron microscopy (TEM), energy dispersive spectroscopy (EDS), and high angle annular dark field scanning TEM (HAADF-STEM) results were obtained using a FEI Talos F200S emission scanning electron microscope, in order to determine the micro-structures of the fabricated composites. Nitrogen adsorption–desorption isotherms

were obtained using a Quantachrome Autosorb iQ-MP-C. Specific surface areas were tested using Brunauer–Emmett–Teller (BET) models. Pore-size distributions were evaluated using Barrett–Joyner–Halenda (BJH) methods.

Electrochemical measurements

The electrochemical measurements were obtained using an electrochemical workstation (CHI660E, CH Instrument) with a standard three-electrode system and 1.0 M KOH solution as the electrolyte. The Hg/HgO electrode, the as-prepared electrode (1×1 cm^2 geometric area), and the graphite electrode were used as the reference, working, and counter electrodes, respectively. Cyclic voltammetry (CV) was performed for 20 cycles at a scan rate of 10 mV s^{-1}. Linear sweep voltammetry (LSV) measurements were performed in a N_2-saturated electrolyte at a scan rate of 5 mV s^{-1}. The measured potentials were calculated as the potential *versus* the reversible hydrogen electrode (RHE) using the equation, $E_{vs.\ RHE} = E_{vs.\ Hg/HgO} + 0.059\ pH + 0.098$. The Tafel slopes were calculated from the LSV polarization curves. For comparison, commercial Pt/C or RuO_2 powders (3 mg) were mixed with a 5 wt% Nafion solution (50 μL), dispersed in ethanol (450 μL) and then sonicated to form a uniform solution. They were then loaded onto bare CC (1×1 cm^2) to form the working electrodes. The electrochemical impedance spectra (EIS) were obtained over a frequency range of 0.01–10^5 Hz. Double-layer capacitance (C_{dl}) data was calculated by cyclic voltammetry (CV) curves between −0.7 to −0.9 V at an increasing sweep rate from 10 to 200 mV s^{-1}. Electrochemical stability measurements were examined by chronopotentiometry curves at the current density of 10 mA cm^{-2} for over 24 h. All measurements were corrected with 85% iR compensation.

Results and discussion

The Co_3O_4@CoWP/CC electrode was prepared in three steps, namely hydrothermal synthesis, phosphidation, and self-assembly processes, as described in Scheme 1. Firstly, cobalt-doped tungsten oxide (CoWO) was precipitated and adhered on a CC surface to form vertically aligned brown-red nanowire arrays of CoWO/CC by hydrothermal treatment. Secondly, the CoWO nanowires were converted to dark blue CoWP nanowires through low-temperature gas-phase phosphidation. The CoWP/CC nanowires could be employed as the support skeleton for the uniform growth and anchoring of an ultrathin layer composed of ultrasmall Co_3O_4 nanoparticles. Finally, cobalt hydroxide precursors were deposited on the surface of the CoWP nanowires by a hydrothermal process, and the ultrathin layer composed of Co_3O_4 nanoparticles was further anchored onto the CoWP/CC nanowires after annealing. The color of the obtained sample turned from dark blue to black, indicating that the cobalt hydroxide had been transformed into Co_3O_4 nanoparticles. The hybrid catalyst with its unique three-dimensional (3-D) hierarchical architecture can facilitate the exposure of catalytic active sites, thereby enhancing the mass/electron mobility and accelerating the diffusion of gaseous products during water electrolysis.

XRD was used to confirm the phase structures of Co_3O_4@CoWP/CC (Fig. 1a), CoWP/CC, and Co_3O_4 (Fig. S1a and b†). The diffraction peaks at 36.8°, 44.8°, and 55.7° could be indexed to the typical (311), (400), and (422) crystal facets of spinel Co_3O_4 (JCPDS no. 42-1467), respectively.[29] In addition, the other main diffraction peaks match well the peaks of orthorhombic WP (JCPDS no. 29-1364),[30] however the main diffraction peak of the (103) plane at $2\theta = 46.5°$ shows a slight positive shift (~0.4°) compared to the standard peak, and this is due to the incorporation of Co atoms into the WP lattice.[31] The XRD results verified the coexistence of Co_3O_4 and CoWP and the formation of the Co_3O_4@CoWP nanohybrid.

XPS was utilized to characterize the elemental valence of Co_3O_4@CoWP/CC, CoWP/CC (Fig. S1c–f†), and Co_3O_4 (Fig. S2a and b†). The survey spectrum in Fig. 1b shows the co-presence of the W, Co, P, and O elements, and the atomic percentages of W, Co, and P of Co_3O_4@CoWP/CC are approximately 4.98%, 1.97%,

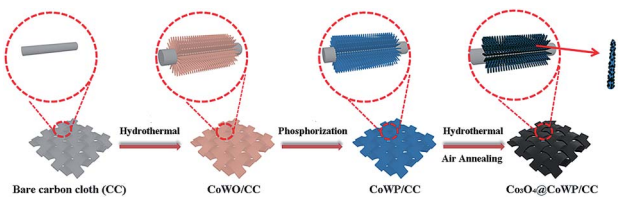

Scheme 1 Illustration of the synthetic route for the Co_3O_4@CoWP/CC electrode.

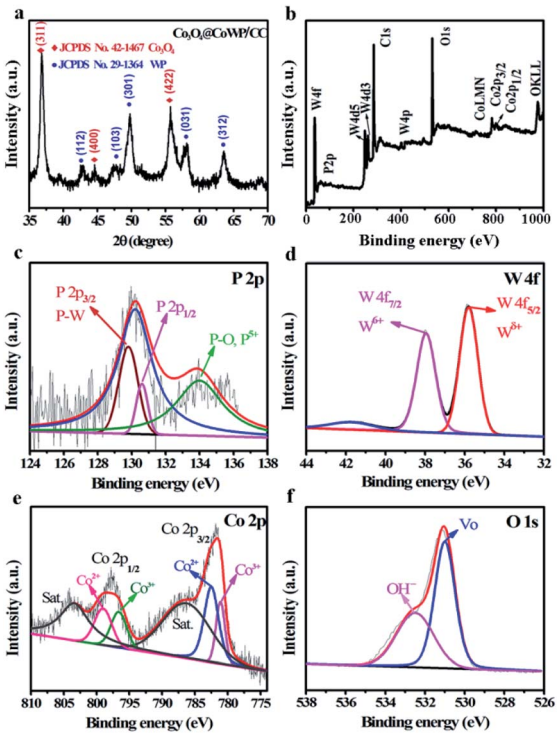

Fig. 1 (a) XRD patterns of the Co_3O_4@CoWP/CC nanohybrid. (b) XPS survey spectrum of Co_3O_4@CoWP/CC and the corresponding high-resolution XPS spectra for (c) P 2p, (d) W 4f, (e) Co 2p, and (f) O 1s.

and 0.96%, respectively. However, the survey spectrum of CoWP/CC (Fig. S1c†) displays a weaker Co 2p peak intensity and has a low Co atomic ratio (~0.8%) for CoWP/CC, confirming the presence of the Co-dopant in CoWP, and this is consistent with the XRD pattern results. The spectrum of the P 2p region in Fig. 1c contains two main peaks. One main peak at 130.0 eV is deconvolved into two peaks including P $2p_{1/2}$ (130.7 eV) and P $2p_{3/2}$ (129.8 eV). The phosphorus species with binding energy at 129.8 eV can be ascribed to the P–W bonds. The other main signal of 134.0 eV can be assigned to the oxidized phosphorus species (P–O) that appears due to surface oxidation.[9] In the W 4f region (Fig. 1d), there are two typical peaks at 37.9 and 35.8 eV that can be associated with W $4f_{7/2}$ and W $4f_{5/2}$, respectively. The W $4f_{7/2}$ peak at 37.9 eV can be assigned to the W^{6+} species, *e.g.* WO_3, and the W $4f_{5/2}$ peak is attributed to $W^{\delta+}$ in CoWP.[32] It can be observed from Fig. 1e that the peaks of Co $2p_{1/2}$ and Co $2p_{3/2}$ are located at approximately 797.5 and 781.5 eV, respectively. The two peaks centered at approximately 787.5 and 804.5 eV are satellite peaks.[33] The Co $2p_{1/2}$ and Co $2p_{3/2}$ peaks are fitted with two spin orbit doublets, indicating the co-presence of Co^{2+} and Co^{3+}. Additionally, the peaks of Co $2p_{1/2}$ and Co $2p_{3/2}$ in Co_3O_4@CoWP show a slight positive shift compared to those of pure-Co_3O_4 (Fig. S2a†), implying tight integration and strong interaction between Co_3O_4 and CoWP.[34] As observed from Fig. 1f, Co_3O_4@CoWP/CC shows two oxygen peaks in the O 1s spectra. In particular, the characteristic peak at 532.5 eV is quite conspicuous, and originates from the hydroxyl species.[26] The other peak at 531.0 eV can be assigned to oxygen vacancies or defects of cobalt oxide that are favorable for improved OER performance.[35] These XPS test results further confirm the preparation of the Co_3O_4@CoWP target product on carbon cloth.

The morphology of the prepared product was further observed by SEM. As shown in Fig. 2a–c, the CoWP nanowires with a regular array structure densely and uniformly cover the entire surface of the carbon cloth. This array structure of the CoWP nanowires does not change and remains perfect in contrast to unphosphorized CoWO/CC, shown in Fig. S3.† The CoWP nanowires were measured to be approximately 1 μm long. The average diameter of the nanowires is 40 nm with a smooth surface and sharp tips, and the diameter decreases gradually from the fixed end to the tip (Fig. 2b and c). When the Co_3O_4 nanoparticles are loaded onto the surface of the CoWP nanowires, the Co_3O_4@CoWP nanowires maintain a perfectly aligned structure, as seen in Fig. 2d–f. The high-magnification SEM image in Fig. 2f shows the increased diameter and rough surface of the Co_3O_4@CoWP nanowires compared with that of CoWP/CC, implying that the ultrathin layer composed of Co_3O_4 nanoparticles is compactly and uniformly anchored onto the exterior surface of the CoWP nanowires. The 3-D Co_3O_4@CoWP nanowire array structure formed on the CC can enlarge the effective surface area for the electrochemical reactions and can facilitate the diffusion of electrolyte between accessible nanowires.

To obtain more detailed information on its structure and composition, Co_3O_4@CoWP was scraped from the carbon cloth and characterized by TEM. The low-magnification image indicates that the length of the Co_3O_4@CoWP nanowires is approximately 1 μm, as shown in Fig. 3a. After the ultrathin layer composed of Co_3O_4 nanoparticles was deposited on the surface of the CoWP nanowires, as shown in Fig. 3b, the Co_3O_4@CoWP nanowires become rougher than the CoWP nanowires (Fig. S4†). Fig. 3c implies that the ultrathin layer that is composed of Co_3O_4 nanoparticles (NPs) is solidly decorated on the CoWP nanowires. The ultrathin layer is about 5 nm thick and consists of uniformly dispersed Co_3O_4 particles. The lattice fringes of CoWP and Co_3O_4 are clearly shown in the HRTEM images presented in Fig. 3d. The lattice spacing of 0.202 nm of CoWP is slightly larger than that of 0.195 nm of WP in the (103) plane (JCPDS no. 29-1364), and this can be attributed to Co-

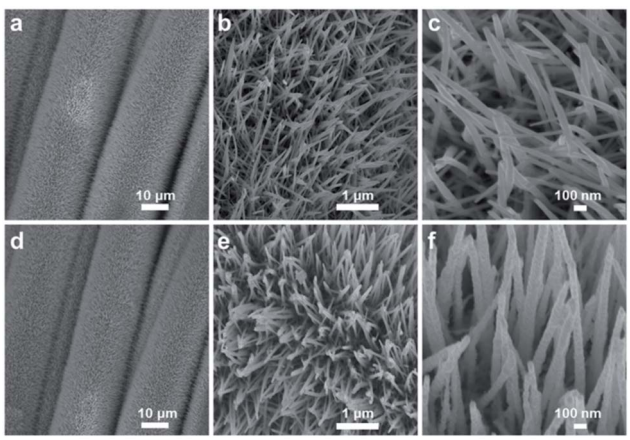

Fig. 2 SEM images of (a–c) the CoWP/CC nanowire array, and (d–f) the Co_3O_4@CoWP/CC nanowire array with different magnifications.

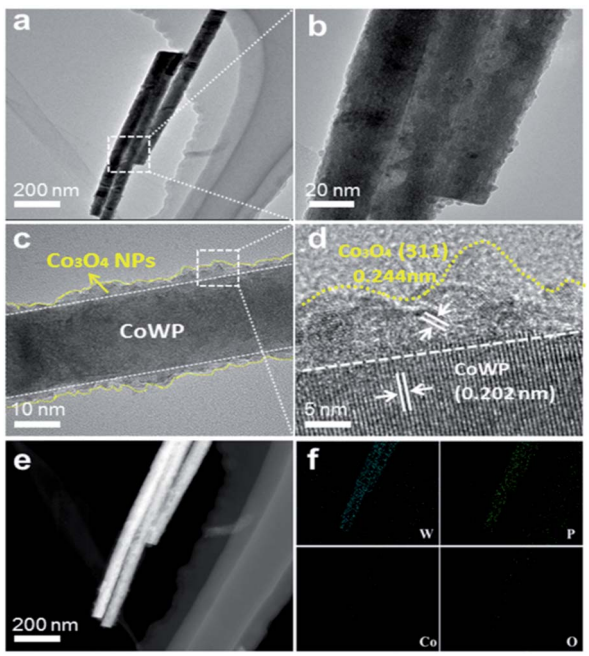

Fig. 3 (a and b) TEM images, (c and d) HRTEM images, and (e and f) HAADF-STEM images with its corresponding element mapping images of Co_3O_4@CoWP/CC.

doping into the crystal lattice of WP.[36,37] The interplanar distances of 0.244 nm are clearly observed, and can be ascribed to the (311) plane of spinel Co_3O_4. These results further verify that the ultrathin layer composed of Co_3O_4 nanoparticles was successfully decorated on the CoWP nanowires, and that the dispersed Co_3O_4 nanoparticles can provide sufficient active sites for the electrochemical reactions.[38]

The EDS results indicate the coexistence of O, Co, P, and W elements in the Co_3O_4@CoWP hybrid, and that these elements are distributed uniformly on the whole nanowire (Fig. 3e and f), which is consistent with the XPS results. Moreover, the EDS spectrum of CoWP also displays the presence of Co, P, and W elements (Fig. S5†). The BET surface areas of Co_3O_4@CoWP/CC and CoWP/CC are 11.80 and 10.85 $m^2\ g^{-1}$ (Fig. S6a†), respectively, demonstrating that the presence of an ultrafine Co_3O_4 nanolayer on CoWP nanowires can appropriately increase the surface area of Co_3O_4@CoWP. The pore-size distribution is mainly found in the 2–7 nm range, as shown in Fig. S6b,† implying mesoporous characteristics of the Co_3O_4@CoWP/CC nanohybrid, and the abundance of mesopores in the structure is beneficial for exposing innumerable catalytically active sites.

The electrocatalytic properties for the OER of the Co_3O_4@CoWP/CC electrode were evaluated using the conventional three-electrode configuration. For comparison, LSV curves of CC-supported CoWP, Co_3O_4, and commercially available RuO_2 were obtained under the same conditions. As illustrated in Fig. 4a, the Co_3O_4@CoWP/CC electrode displays good electrocatalytic OER ability with an overpotential (η_{10}) of 269 mV at the current density of 10 mA cm^{-2}, and this is clearly lower than those of CoWP/CC (311 mV) and Co_3O_4/CC (327 mV) and is only slightly higher than that of RuO_2 (211 mV). As the highly dispersed Co_3O_4 nanoparticles are modified on the surface of the CoWP nanowires, Co atoms can effectively provide more active reaction sites for hydroxyl adsorption, so the OER performance is significantly improved.[39]

The Tafel slope is an important metric to evaluate electrocatalyst performance, and a smaller Tafel slope usually means that the electrocatalyst needs a lower overpotential to gain the identical current density. Accordingly, the Tafel slopes of Co_3O_4@CoWP/CC, CoWP/CC, Co_3O_4/CC, and bare CC for the OER were obtained and were 69, 82, 90, and 106 mV dec^{-1} (Fig. 4b), respectively, demonstrating the faster OER reaction kinetics and accelerated electron transfer transport ability on the Co_3O_4@CoWP composite interface.[38]

EIS was implemented to investigate the kinetics of mass transport and the conductivity of the electrodes. Nyquist plots for Co_3O_4@CoWP/CC, CoWP/CC, and Co_3O_4/CC were obtained through equivalent fitting, as shown in Fig. 4c, in which the Co_3O_4@CoWP/CC electrode had the smallest charge transfer resistance (R_{ct}) among the tested samples. Benefiting from the synergy between the highly ordered array of CoWP nanowires and the uniformly dispersed Co_3O_4 fine nanoparticles, the charge transfer resistance between CoWP and Co_3O_4 is reduced.[40]

Moreover, the electrochemically active surface area (ECSA) is necessary evidence to explore the difference in the natural electrocatalytic activity. According to the reported method, the

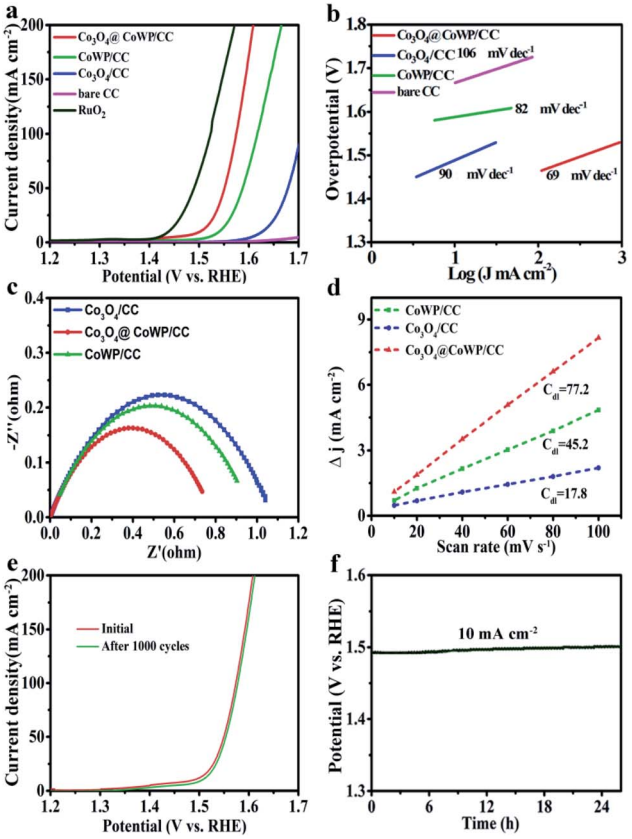

Fig. 4 OER performances of the catalysts in alkaline media. (a) Polarization curves of Co_3O_4@CoWP/CC, CoWP/CC, and Co_3O_4/CC. (b) Tafel slopes and (c) EIS curves of the electrocatalysts at an overpotential of 10 mV. (d) Calculated electrochemical C_{dl} values for the corresponding electrocatalysts. (e) Polarization curves of Co_3O_4@CoWP/CC before (initial) and after 1000 cycling tests. (f) Chronopotentiometric measurement of Co_3O_4@CoWP/CC for 24 h at 10 mA cm^{-2}.

CV results obtained at different scan rates (Fig. S7†) were used to calculate C_{dl}.[41] As can be seen from Fig. 4d, the C_{dl} values of Co_3O_4/CC, CoWP/CC, and Co_3O_4@CoWP/CC are 17.8, 45.2, and 77.2 mF cm^{-2}, respectively. The Co_3O_4@CoWP/CC electrode has the largest C_{dl} value, indicating its highest effective electrochemically active area with abundant active sites exposed for the OER.[42]

The Co_3O_4 nanoparticles are mainly responsible for the effective electrocatalysis of water oxidation, while CoWP/CC provides a conductive structural support for electron transport and generates catalytic synergy. The possible cobalt oxide-catalyzed reactions can generally be expressed as eqn (1) and (2).

$$Co_3O_4 + H_2O + OH^- \rightarrow 3CoOOH + e^- \quad (1)$$

$$CoOOH + OH^- \rightarrow CoO_2 + H_2O + e^- \quad (2)$$

In this process, the reaction of CoOOH with CoO_2 is the rate-determining step, and Co(IV) is considered to be the active species of the OER. In addition, OH^- reacts with CoO_2 to generate adsorbed H_2O_2. Then, H_2O_2 decomposes to produce

the HOO species that subsequently reacts with OH^-, leading to the formation of H_2O and O_2, accompanied by the release of an electron.[43,44]

Since stability and durability are important factors that must be considered in practical applications, long-term CV scanning was performed in an alkaline environment. After 1000 cycling tests, the polarization curve for Co_3O_4@CoWP/CC showed negligible change for the OER overpotential relative to the initial curve (Fig. 4e), indicating that the Co_3O_4@CoWP/CC electrode has superior stability in long-term electrocatalytic processes. The chronopotentiometry measurement was also performed for more than 24 h, as shown in Fig. 4f. The electrocatalytic activity decreased slightly after continuous operation, further elucidating the superb durability of the catalyst. This result revealed that the integration of the catalytic active component (Co_3O_4 nanoparticles) with the conductive and robust substrate (CoWP/CC) can generate a synergistic effect for the OER, resulting in high ionic/electric conductivity, excellent chemical/mechanical stability, and rapid mass-transport.

The HER activity was tested in alkaline media at a scan rate of 5 mV s^{-1}. The measured LSV curves of different electrocatalysts are summarized in Fig. 5a. The Co_3O_4@CoWP/CC nanohybrid electrode exhibits improved HER performance with η_{10} of 118 mV, and this exceeds most tungsten-based catalysts under alkaline conditions. For comparison, in order to achieve identical current density, CoWP/CC, Co_3O_4/CC, and commercial Pt/C require overpotentials of 269, 460, and 51 mV, respectively. Compared with pure-CoWP and pure-Co_3O_4, Co partial substitution for W in WP and the interface between Co_3O_4 and CoWP may introduce P defects in Co_3O_4@CoWP.[45] The existence of P defects is conducive to H_2O dissociation, and thus improves the HER activity in an alkaline environment. At the same time, the energy barrier for H_2 production also decreases by Co-doping. Thus, both water dissociation and hydrogen release are significantly accelerated on Co-WP.[46,47] Tafel slopes in Fig. 5b show the reaction kinetics information of the as-synthesized catalyst. The Tafel slopes of Co_3O_4@CoWP/CC, CoWP/CC, Co_3O_4/CC, and bare CC for HER are 58, 94, 177, and 194 mV dec^{-1}, respectively. The lowest value for the Co_3O_4@CoWP/CC electrode proves that the catalytic HER process of the target nanohybrid follows the Volmer–Heyrovsky mechanism.[48] Highly dispersed Co_3O_4 ultrafine nanoparticles with numerous active sites are integrated with the highly conductive CoWP/CC nanowire array to obtain a 3-D layered configuration that effectively promotes HER kinetics. Moreover, the stability and long-term test results are shown in Fig. 5c. After the 2000th cycle, the LSV curve deviates slightly from that of the 1st cycle. This verifies that the catalyst is highly stable in the electrochemical HER reaction. Similarly, after 24 h of continuous operation (Fig. 5d), a relatively small reduction in the HER overpotential was observed. These results show the superior hydrogen evolution stability and durability of the catalyst. Overall, Co-doping optimizes and stabilizes the nanowire structure of WP, and then cooperates with the Co_3O_4 nanoparticles, thus achieving impressively high electrocatalytic activity for HER and excellent stability of the catalyst. The excellent stability can be confirmed from the TEM images, XRD patterns, and EDS data of Co_3O_4@CoWP/CC after 24 h of continuous electrolyzing at 10 mA cm^{-2} for the HER (Fig. S8 and S9†). The microstructures, phase structure and compositions of the ultrafine Co_3O_4 nanolayer shelled CoWP nanowire are well maintained after the HER reaction.

Inspired by the good OER and HER performances, the Co_3O_4@CoWP/CC hybrid material was further applied as a bifunctional electrocatalyst (denoted as Co_3O_4@CoWP/CC||Co_3O_4@CoWP/CC) for overall water splitting in a two-

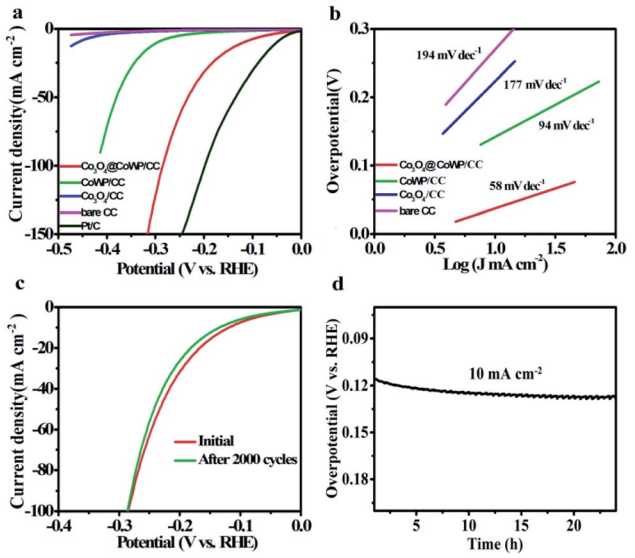

Fig. 5 HER performances of the catalysts in alkaline media. (a) LSV curves of Co_3O_4@CoWP/CC, CoWP/CC, and Co_3O_4/CC. (b) Tafel slopes and (c) polarization curves of Co_3O_4@CoWP/CC before (initial) and after 2000 cycles. (d) Chronopotentiometric measurement of Co_3O_4@CoWP/CC for 24 h at 10 mA cm^{-2}.

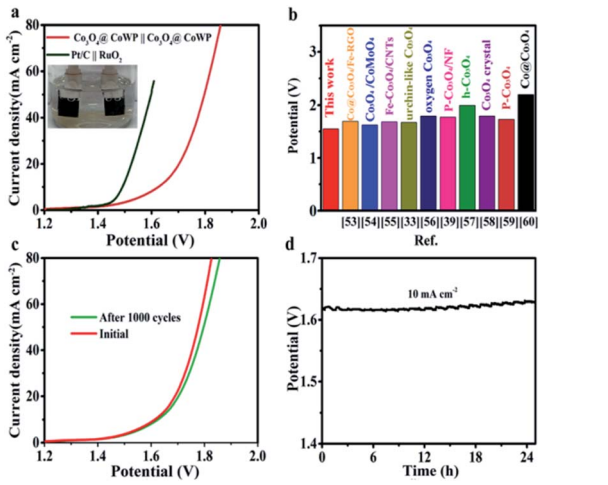

Fig. 6 (a) LSV curves of water splitting in a two-electrode system (inset: the optical photograph of the generation of gases). (b) Cell voltages required to achieve a current density of 10 mA cm^{-2} for overall water splitting. (c) Polarization curves before (initial) and after 1000 cycling tests. (d) Chronoamperometry curve at 10 mA cm^{-2}. All tests were performed in alkaline media.

Table 1 Comparison of OER and HER activities for Co_3O_4@CoWP/CC with other reported bifunctional electrocatalysts in 1.0 M KOH

Catalysts	Overpotential (mV) at 10 mA cm^{-2}		Two-electrode $E(V)$ at 10 mA cm^{-2}	Ref.
	OER	HER		
Co_3O_4@MoS_2	269	207	1.59	3
WP NAs/CC	—	150	—	9
Co-WP	—	119	—	46
Co@Co_3O_4/FeNS-RGO	287	130	1.65	53
Co_3O_4/$CoMoO_4$	244	143	1.61	54
Co@Co_3O_4-NC	391	221	2.00	60
CoWP@(S,N)–C	430	61	—	61
CoP/NF	281	95	1.61	62
ZIF@LDH@NF	318	106	1.59	63
Co_3O_4@CoWP/CC	269	118	1.61	This work

electrode configuration. As can be clearly seen in Fig. 6a, the Co_3O_4@CoWP/CC cell exhibits slightly inferior performance to that of the Pt/C||RuO_2 cell (cell potential 1.49 V at 10 mA cm^{-2}) with a cell potential of 1.61 V at 10 mA cm^{-2}, however this performance is much better than those of the most reported cobalt oxide bifunctional water splitting electrocatalysts, as illustrated in Fig. 6b.[55–59] Furthermore, a comparison of electrocatalytic activity for the recently reported bifunctional catalysts is illustrated in Table 1. After 1000 CV cycles, the overall water electrolysis still shows good activity (Fig. 6c). The chronoamperometry curve at a constant current density shows no apparent degradation for over 24 h (Fig. 6d). Therefore, Co_3O_4@CoWP/CC exhibits excellent and stable electrocatalytic performance for overall water splitting. The significantly improved electrocatalytic properties can be attributed to the optimized structural characteristics, including the numerous exposed metal active sites due to the ultrafine Co_3O_4 nanoparticles, the improved electrical conductivity of the hierarchical architecture, and the strong synergistic effect between Co_3O_4 and CoWP.

Based on the above results, the as-prepared Co_3O_4@CoWP/CC electrocatalyst displays enhanced water electrolysis. The reasons for this can be described as follows: (i) the affinity of CoWP and Co_3O_4 can promote the electrolytic reaction of water. In the OER process, the homogeneous and stable coverage of the ultrafine Co_3O_4 nanolayer on the nanowires forms step sites or dislocations,[14] increasing the active surface area of the electrode, providing more reactive sites, and enhancing the adsorption of the oxygen intermediates.[49,50] In the HER process, the Co-doping in CoWP exhibits a coordinative effect, enhancing water dissociation and optimizing hydrogen adsorption/desorption, and this consequently facilitates all of the HER steps in alkaline solutions.[45–47] (ii) Due to the synergistic interactions (such as higher conductivity, good electron/mass transport, high mechanical strength, and excellent catalytic stability) between the highly conductive CoWP/CC matrix and the ultrafine Co_3O_4 nanolayer, the peculiar hierarchical 3-D structure exhibits superior electrocatalytic water splitting performance. (iii) The free-standing growth of the catalyst on the conductive substrate avoids the use of a post-coating process and the addition of a binder. The array nanowires with open space facilitate the penetration of the electrolyte and the diffusion of electron/ionic species, resulting in the high utilization efficiency of the active ingredients.[51,52] Therefore, such integration of heterogeneous assembly induces significantly enhanced OER and HER activities, leading to a highly efficient bifunctional catalyst for alkaline water electrolysis.

Conclusions

In conclusion, we constructed a 3D Co_3O_4@CoWP hybrid grown on carbon cloth as an active and robust bifunctional electrocatalyst for alkaline water electrolysis. The obtained Co_3O_4@CoWP/CC electrode shows impressive catalytic activities for the OER (η_{10} = 269 mV) and HER (η_{10} = 118 mV). An alkaline electrolyzer of Co_3O_4@CoWP/CC requires a cell voltage of only 1.61 V to deliver a current density of 10 mA cm^{-2}, and this is more active than most reported non-metal electrocatalysts. The improved overall water splitting ability can be ascribed to the unique nanostructure that provides not only sufficient active sites for the electrode reactions, but also suitable routes for the transport of ions, electrons, and gas molecules, as well as the synergistic interactions between CoWP and the surface-modified ultrathin layer that is composed of Co_3O_4 nanoparticles, which facilitates the catalytic reaction kinetics. This work provides additional hopeful prospects for the development of highly efficient, stable, and low-cost catalysts that contain non-noble metals for electrochemical overall water electrolysis.

Conflicts of interest

There are no conflicts to declare.

Acknowledgements

This work was supported by the National Natural Science Foundation of China (Grants U1804140, U21978021, and 21706242) and the Fundamental Research Funds for the Central Universities. The authors gratefully acknowledge the Center for

Advanced Analysis and Gene Sequencing of Zhengzhou University.

Notes and references

1 Y. Wang, R. K. Hocking, W. Adamson and C. Zhao, Overall electrochemical splitting of water at the heterogeneous interface of nickel and iron oxide, *Nat. Commun.*, 2019, **10**, 1–10.

2 J. Yang, D. Guo, S. Zhao, Y. Lin, R. Yang, D. Xu, N. Shi, X. Zhang, L. Lu, Y. Q. Lan, J. Bao and M. Han, *Small*, 2019, **15**, 1–12.

3 J. Liu, J. Wang, B. Zhang, Y. Ruan, H. Wan, X. Ji, K. Xu, D. Zha, L. Miao and J. Jiang, *J. Mater. Chem. A*, 2018, **6**, 2067–2072.

4 Y. H. Chung, I. Jang, J. H. Jang, H. S. Park, H. C. Ham, J. H. Jang, Y. K. Lee and S. J. Yoo, Anomalous *in situ* activation of carbon-supported Ni_2P nanoparticles for oxygen evolving electrocatalysis in alkaline media, *Sci. Rep.*, 2017, **7**, 1–8.

5 C. Zhu, Q. Shi, S. Feng, D. Du and Y. Lin, Single-atom catalysts for electrochemical water splitting, *ACS Energy Lett.*, 2018, **3**, 1713–1721.

6 Q. Zhang, N. M. Bedford, J. Pan, X. Lu and R. Amal, A fully reversible water electrolyzer cell made up from FeCoNi (oxy) hydroxide atomic layers, *Adv. Energy Mater.*, 2019, **9**, 1–13.

7 D. Lyu, Y. Du, S. Huang, B. Y. Mollamahale, X. Zhang, S. W. Hasan, F. Yu, S. Wang, Z. Q. Tian and P. K. Shen, Highly efficient multifunctional Co–N–C electrocatalysts with synergistic effects of Co–N moieties and Co metallic nanoparticles encapsulated in a N-doped carbon matrix for water-splitting and oxygen redox reactions, *ACS Appl. Mater. Interfaces*, 2019, **11**, 39809–39819.

8 Q. Liang, H. Jin, Z. Wang, Y. Xiong, S. Yuan, X. Zeng, D. He and S. Mu, Metal-organic frameworks derived reverse-encapsulation Co-NC@Mo_2C complex for efficient overall water splitting, *Nano Energy*, 2019, **57**, 746–752.

9 Z. Pu, Q. Liu, A. M. Asiri and X. Sun, Tungsten phosphide nanorod arrays directly grown on carbon cloth: a highly efficient and stable hydrogen evolution cathode at all pH values, *ACS Appl. Mater. Interfaces*, 2014, **6**, 21874–21879.

10 E. J. Popczun, J. R. McKone, C. G. Read, A. J. Biacchi, A. M. Wiltrout, N. S. Lewis and R. E. Schaak, Nanostructured nickel phosphide as an electrocatalyst for the hydrogen evolution reaction, *J. Am. Chem. Soc.*, 2013, **135**, 9267–9270.

11 Q. Liu, J. Tian, W. Cui, P. Jiang, N. Cheng, A. M. Asiri and X. Sun, Carbon nanotubes decorated with CoP nanocrystals: A highly active non-noble-metal nanohybrid electrocatalyst for hydrogen evolution, *Angew. Chem., Int. Ed.*, 2014, **53**, 6710–6714.

12 P. Xiao, M. A. Sk, L. Thia, X. Ge, R. J. Lim, J. Y. Wang, K. H. Lim and X. Wang, Molybdenum phosphide as an efficient electrocatalyst for the hydrogen evolution reaction, *Energy Environ. Sci.*, 2014, **7**, 2624–2629.

13 P. Jiang, Q. Liu, Y. Liang, J. Tian, A. M. Asiri and X. Sun, A cost-effective 3D hydrogen evolution cathode with high catalytic activity: FeP nanowire array as the active phase, *Angew. Chem., Int. Ed.*, 2014, **53**, 12855–12859.

14 J. Tian, Q. Liu, N. Cheng, A. M. Asiri and X. Sun, Self-supported Cu_3P nanowire arrays as an integrated high-performance three-dimensional cathode for generating hydrogen from water, *Angew. Chem., Int. Ed.*, 2014, **53**, 9577–9581.

15 M. Pi, T. Wu, D. Zhang, S. Chen and S. Wang, Self-supported three-dimensional mesoporous semimetallic WP_2 nanowire arrays on carbon cloth as a flexible cathode for efficient hydrogen evolution, *Nanoscale*, 2016, **8**, 19779–19786.

16 Z. Cai, A. Wu, H. Yan, Y. Xiao, C. Chen, C. Tian, L. Wang, R. Wang and H. Fu, Hierarchical whisker-on-sheet NiCoP with adjustable surface structure for efficient hydrogen evolution reaction, *Nanoscale*, 2018, **10**, 7619–7629.

17 J. Tian, Q. Liu, A. M. Asiri and X. Sun, Self-supported nanoporous cobalt phosphide nanowire arrays: an efficient 3D hydrogen-evolving cathode over the wide range of pH 0–14, *J. Am. Chem. Soc.*, 2014, **136**, 7587–7590.

18 C. Tang, R. Zhang, W. Lu, L. He, X. Jiang, A. M. Asiri and X. Sun, Fe-doped CoP nanoarray: a monolithic multifunctional catalyst for highly efficient hydrogen generation, *Adv. Mater.*, 2017, **29**, 1602441.

19 D. Jiang, Y. Xu, R. Yang, D. Li, S. Meng and M. Chen, CoP_3/CoMoP heterogeneous nanosheet arrays as robust electrocatalyst for pH-universal hydrogen evolution reaction, *ACS Sustainable Chem. Eng.*, 2019, **7**, 9309–9317.

20 Z. Ren, X. Ren, L. Zhang, C. Fu, X. Li, Y. Zhang, B. Gao, L. Yang, P. K. Chu and K. Huo, Tungsten-doped CoP nanoneedle arrays grown on carbon cloth as efficient bifunctional electrocatalysts for overall water splitting, *ChemElectroChem*, 2019, **6**, 5229–5236.

21 A. Mendoza-Garcia, H. Zhu, Y. Yu, Q. Li, L. Zhou, D. Su, M. J. Kramer and S. Sun, Controlled anisotropic growth of Co-Fe-P from Co-Fe-O nanoparticles, *Angew. Chem., Int. Ed.*, 2015, **54**, 9642–9645.

22 J. Li, M. Yan, X. Zhou, Z. Q. Huang, Z. Xia, C. R. Chang, Y. Ma and Y. Qu, Mechanistic insights on ternary $Ni_{2-x}Co_xP$ for hydrogen evolution and their hybrids with graphene as highly efficient and robust catalysts for overall water splitting, *Adv. Funct. Mater.*, 2016, **26**, 6785–6796.

23 J. Liu, J. Wang, B. Zhang, Y. Ruan, L. Lv, X. Ji, K. Xu, L. Miao and J. Jiang, Hierarchical $NiCo_2S_4$@NiFe LDH heterostructures supported on nickel foam for enhanced overall-water-splitting activity, *ACS Appl. Mater. Interfaces*, 2017, **9**, 15364–15372.

24 Y. Guo, J. Tang, Z. Wang, Y. M. Kang, Y. Bando and Y. Yamauchi, Elaborately assembled metal sulfides as a bifunctional core–shell structured catalyst for highly efficient electrochemical overall water splitting, *Nano Energy*, 2018, **47**, 494–502.

25 J. Saha, R. Ball, A. Sah, V. Kalyani and C. Subramaniam, The mechanistic role of a support-catalyst interface in electrocatalytic water reduction by Co_3O_4 supported nanocarbon florets, *Nanoscale*, 2019, **11**, 13532–13540.

26 T. Chen, S. Li, L. Ma, X. Zhao and G. Fang, Aldehyde reduced Co_3O_4 to form oxygen vacancy and enhance the electrochemical performance for oxygen evolution reaction and supercapacitors, *Nanotechnology*, 2019, **30**, 395403.

27 S. S. Jayaseelan and N. Bhuvanendran, Co_3O_4 nanoparticles decorated polypyrrole/carbon nanocomposite as efficient bi-functional electrocatalyst for electrochemical water splitting, *Int. J. Hydrogen Energy*, 2020, **45**, 4587–4595.

28 J. Wu, Y. Xue, X. Yan, W. Yan, Q. Cheng and Y. Xie, Co_3O_4 nanocrystals on single-walled carbon nanotubes as a highly efficient oxygen-evolving catalyst, *Nano Res.*, 2012, **5**, 521–530.

29 S. Yang, Y. Liu, Y. Hao, X. Yang, W. A. Goddard, X. L. Zhang and B. Cao, Oxygen-vacancy abundant ultrafine Co_3O_4/graphene composites for high-rate supercapacitor electrodes, *Adv. Sci.*, 2018, **5**, 1700659.

30 Y. Duan, Y. Sun, S. Pan, Y. Dai, L. Hao and J. Zou, Self-Stable WP/C Support with excellent cocatalytic functionality for Pt: enhanced catalytic activity and durability for methanol electro-oxidation, *ACS Appl. Mater. Interfaces*, 2016, **8**, 33572–33582.

31 Y. Tan, H. Wang, P. Liu, Y. Shen, C. Cheng, A. Hirata, T. Fujita, Z. Tang and M. Chen, Versatile nanoporous bimetallic phosphides towards electrochemical water splitting, *Energy Environ. Sci.*, 2016, **9**, 2257–2261.

32 H. Zhou, G. Ran, J. F. Masson, C. Wang, Y. Zhao and Q. Song, Novel tungsten phosphide embedded nitrogen-doped carbon nanotubes: a portable and renewable monitoring platform for anticancer drug in whole blood, *Biosens. Bioelectron.*, 2018, **105**, 226–235.

33 R. Li, D. Zhou, J. Luo, W. Xu, J. Li, S. Li, P. Cheng and D. Yuan, The urchin-like sphere arrays Co_3O_4 as a bifunctional catalyst for hydrogen evolution reaction and oxygen evolution reaction, *J. Power Sources*, 2017, **341**, 250–256.

34 T. Y. Ma, S. Dai, M. Jaroniec and S. Z. Qiao, Metal-organic framework derived hybrid Co_3O_4-carbon porous nanowire arrays as reversible oxygen evolution electrodes, *J. Am. Chem. Soc.*, 2014, **136**, 13925–13931.

35 W. Xu, F. Lyu, Y. Bai, A. Gao, J. Feng, Z. Cai and Y. Yin, Porous cobalt oxide nanoplates enriched with oxygen vacancies for oxygen evolution reaction, *Nano Energy*, 2018, **43**, 110–116.

36 C. Tang, L. Gan, R. Zhang, W. Lu, X. Jiang, A. M. Asiri, X. Sun, J. Wang and L. Chen, Ternary $Fe_xCo_{1-x}P$ nanowire array as a robust hydrogen evolution reaction electrocatalyst with Pt-like activity: experimental and theoretical insight, *Nano Lett.*, 2016, **16**, 6617–6621.

37 H. Du, L. Xia, S. Zhu, F. Qu and F. Qu, Al-doped Ni_2P nanosheet array: a superior and durable electrocatalyst for alkaline hydrogen evolution, *Chem. Commun.*, 2018, **54**, 2894–2897.

38 X. Han, X. Wu, C. Zhong, Y. Deng, N. Zhao and W. Hu, $NiCo_2S_4$ nanocrystals anchored on nitrogen-doped carbon nanotubes as a highly efficient bifunctional electrocatalyst for rechargeable zinc-air batteries, *Nano Energy*, 2017, **31**, 541–550.

39 Z. Wang, H. Liu, R. Ge, X. Ren, J. Ren, D. Yang, L. Zhang and X. Sun, Phosphorus-doped Co_3O_4 nanowire array: a highly efficient bifunctional electrocatalyst for overall water splitting, *ACS Catal.*, 2018, **8**, 2236–2241.

40 Y. Zhong, Z. Pan, X. Wang, J. Yang, Y. Qiu and S. Xu, Hierarchical Co_3O_4 nano-micro arrays featuring superior activity as cathode in a flexible and rechargeable zinc-air battery, *Adv. Sci.*, 2019, **6**, 1802243.

41 M. Li, Y. Zhu, H. Wang, C. Wang, N. Pinna and X. Lu, Ni strongly coupled with Mo_2C encapsulated in nitrogen-doped carbon nanofibers as robust bifunctional catalyst for overall water splitting, *Adv. Energy Mater.*, 2019, **9**, 1–11.

42 S. Li, S. Sirisomboonchai, A. Yoshida, X. An, X. Hao, A. Abudula and G. Guan, Bifunctional CoNi/$CoFe_2O_4$/Ni foam electrodes for efficient overall water splitting at a high current density, *J. Mater. Chem. A*, 2018, **6**, 19221–19230.

43 J. A. Koza, Z. He, A. S. Miller and J. A. Switzer, Electrodeposition of crystalline Co_3O_4 – a catalyst for the oxygen evolution reaction, *Chem. Mater.*, 2012, **24**, 3567–3573.

44 N. H. Chou, P. N. Ross, A. T. Bell and T. D. Tilley, Comparison of cobalt-based nanoparticles as electrocatalysts for water oxidation, *ChemSusChem*, 2011, **4**, 1566–1569.

45 X. Huang, X. Xu, X. Luan and D. Cheng, CoP nanowires coupled with CoMoP nanosheets as a highly efficient cooperative catalyst for hydrogen evolution reaction, *Nano Energy*, 2020, **68**, 104332.

46 J. Wang, K. Chang, Z. Sun, J. H. Lee, B. M. Tackett, C. Zhang, J. G. Chen and C. J. Liu, A combined experimental and theoretical study of the accelerated hydrogen evolution kinetics over wide pH range on porous transition metal doped tungsten phosphide electrocatalysts, *Appl. Catal., B*, 2019, **251**, 162–167.

47 X. D. Wang, Y. F. Xu, H. S. Rao, W. J. Xu, H. Y. Chen, W. X. Zhang, D. Bin Kuang and C. Y. Su, Novel porous molybdenum tungsten phosphide hybrid nanosheets on carbon cloth for efficient hydrogen evolution, *Energy Environ. Sci.*, 2016, **9**, 1468–1475.

48 P. Wang, X. Zhang, J. Zhang, S. Wan, S. Guo, G. Lu, J. Yao and X. Huang, Precise tuning in platinum–nickel/nickel sulfide interface nanowires for synergistic hydrogen evolution catalysis, *Nat. Commun.*, 2017, **8**, 1–9.

49 A. Nairan, P. Zou, C. Liang, J. Liu, D. Wu, P. Liu and C. Yang, NiMo solid solution nanowire array electrodes for highly efficient hydrogen evolution reaction, *Adv. Funct. Mater.*, 2019, **29**, 1–8.

50 H. Zhou, F. Yu, Y. Huang, J. Sun, Z. Zhu, R. J. Nielsen, R. He, J. Bao, W. A. Goddard, S. Chen and Z. Ren, Efficient hydrogen evolution by ternary molybdenum sulfoselenide particles on self-standing porous nickel diselenide foam, *Nat. Commun.*, 2016, **7**, 1–7.

51 X. D. Wang, H. Y. Chen, Y. F. Xu, J. F. Liao, B. X. Chen, H. S. Rao, D. Bin Kuang and C. Y. Su, Self-supported $NiMoP_2$ nanowires on carbon cloth as an efficient and

durable electrocatalyst for overall water splitting, *J. Mater. Chem. A*, 2017, **5**, 7191–7199.

52 S. Li, W. Zang, X. Liu, S. J. Pennycook and Z. Kou, Heterojunction engineering of $MoSe_2/MoS_2$ with electronic modulation towards synergetic hydrogen evolution reaction and supercapacitance performance, *Chem. Eng. J.*, 2019, **359**, 1419–1426.

53 J. Zhu, W. Tu, Z. Bai, H. Pan, P. Ji, H. Zhang, Z. Deng and H. Zhang, Zeolitic-imidazolate-framework-derived $Co@Co_3O_4$ embedded into iron, nitrogen, sulfur Co-doped reduced graphene oxide as efficient electrocatalysts for overall water splitting and zinc-air batteries, *Electrochim. Acta*, 2019, **323**, 134821.

54 Z. Pei, L. Xu and W. Xu, Hierarchical honeycomb-like Co_3O_4 pores coating on $CoMoO_4$ nanosheets as bifunctional efficient electrocatalysts for overall water splitting, *Appl. Surf. Sci.*, 2018, **433**, 256–263.

55 H. Begum and S. Jeon, Highly efficient and stable bifunctional electrocatalyst for water splitting on Fe–Co_3O_4/carbon nanotubes, *Int. J. Hydrogen Energy*, 2018, **43**, 5522–5529.

56 G. Cheng, T. Kou, J. Zhang, C. Si, H. Gao and Z. Zhang, O_2^{2-}/O^- functionalized oxygen-deficient Co_3O_4 nanorods as high performance supercapacitor electrodes and electrocatalysts towards water splitting, *Nano Energy*, 2017, **38**, 155–166.

57 Y. P. Zhu, T. Y. Ma, M. Jaroniec and S. Z. Qiao, Self-templating synthesis of hollow Co_3O_4 microtube arrays for highly efficient water electrolysis, *Angew. Chem., Int. Ed.*, 2017, **56**, 1324–1328.

58 S. Du, Z. Ren, J. Zhang, J. Wu, W. Xi, J. Zhu and H. Fu, Co_3O_4 nanocrystal ink printed on carbon fiber paper as a large-area electrode for electrochemical water splitting, *Chem. Commun.*, 2015, **51**, 8066–8069.

59 Z. Xiao, Y. Wang, Y. C. Huang, Z. Wei, C. L. Dong, J. Ma, S. Shen, Y. Li and S. Wang, Filling the oxygen vacancies in Co_3O_4 with phosphorus: an ultra-efficient electrocatalyst for overall water splitting, *Energy Environ. Sci.*, 2017, **10**, 2563–2569.

60 C. Bai, S. Wei, D. Deng, X. Lin, M. Zheng and Q. Dong, A nitrogen-doped nano carbon dodecahedron with $Co@Co_3O_4$ implants as a bi-functional electrocatalyst for efficient overall water splitting, *J. Mater. Chem. A*, 2017, **5**, 9533–9536.

61 B. Weng, C. R. Grice, W. Meng, L. Guan, F. Xu, Y. Yu, C. Wang, D. Zhao and Y. Yan, Metal-organic framework-derived CoWP@C composite nanowire electrocatalyst for efficient water splitting, *ACS Energy Lett.*, 2018, **3**, 1434–1442.

62 P. Wang, F. Song, R. Amal, Y. H. Ng and X. Hu, Efficient water splitting catalyzed by cobalt phosphide-based nanoneedle arrays supported on carbon cloth, *ChemSusChem*, 2016, **9**, 472–477.

63 Y. Tang, X. Fang, X. Zhang, G. Fernandes, Y. Yan, D. Yan, X. Xiang and J. He, Space-confined earth-abundant bifunctional electrocatalyst for high-efficiency water splitting, *ACS Appl. Mater. Interfaces*, 2017, **9**, 36762–36771.